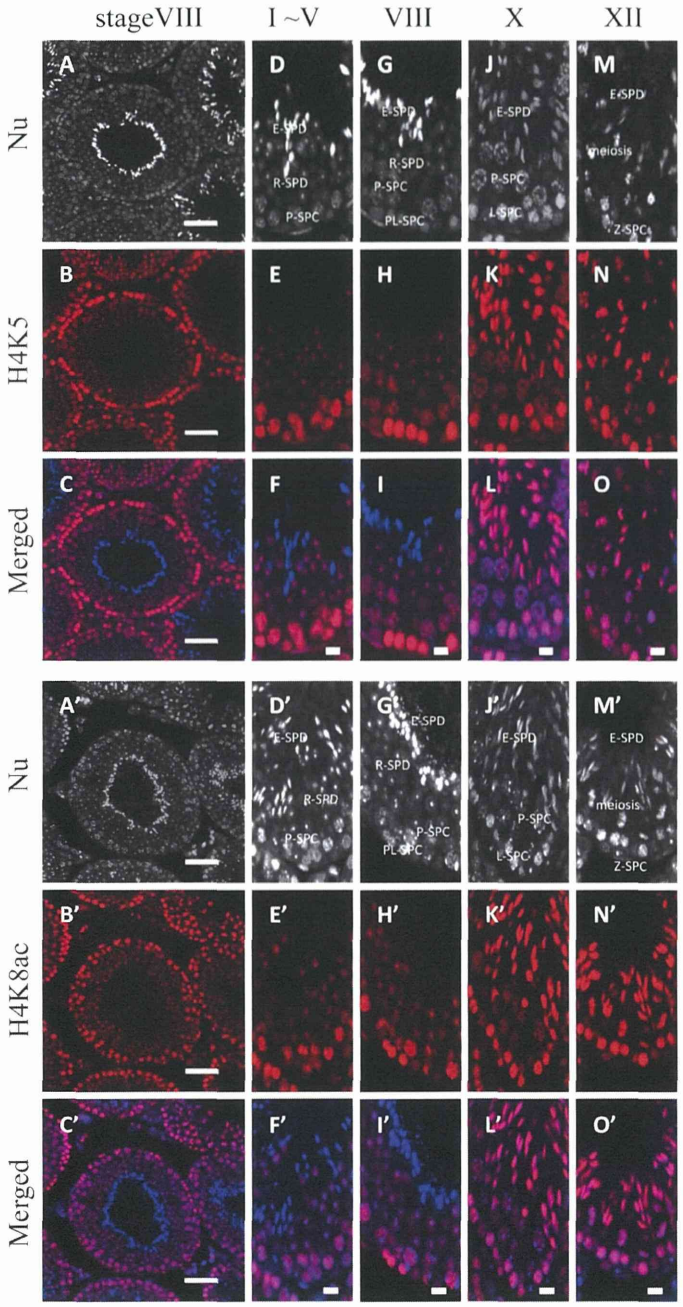

Fig. 1. Immunohistochemical analysis of H4K5ac and H4K8ac. The signals represent nuclear (A, A', D, D', G, G', J, J', M, M') histone H4 lysine 5 acetylation (H4K5ac) (B, E, H, K, N) and histone H4 lysine 8 acetylation (H4K8ac) (B', E', H', K', N'). Stage VIII seminiferous tubules are shown (A– C, A'–C') (G–I, G'–I'). Stage I–V (D–F, D'–F'), stage X (J–L, J'–L') and stage XII (M–O, M'–O') seminiferous tubules are shown. The scale bars represent 50 μm (A, A', B, B', C, C') and 10 μm (F, F', I, I', L, L', O, O'). P-SPC, pachytene spermatocyte; PL-SPC, preleptotene spermatocyte; L-SPC, leptotene spermatocyte; Z-SPC, zygotene spermatocyte; R-SPD, round spermatid; and E-SPD, elongated spermatid.

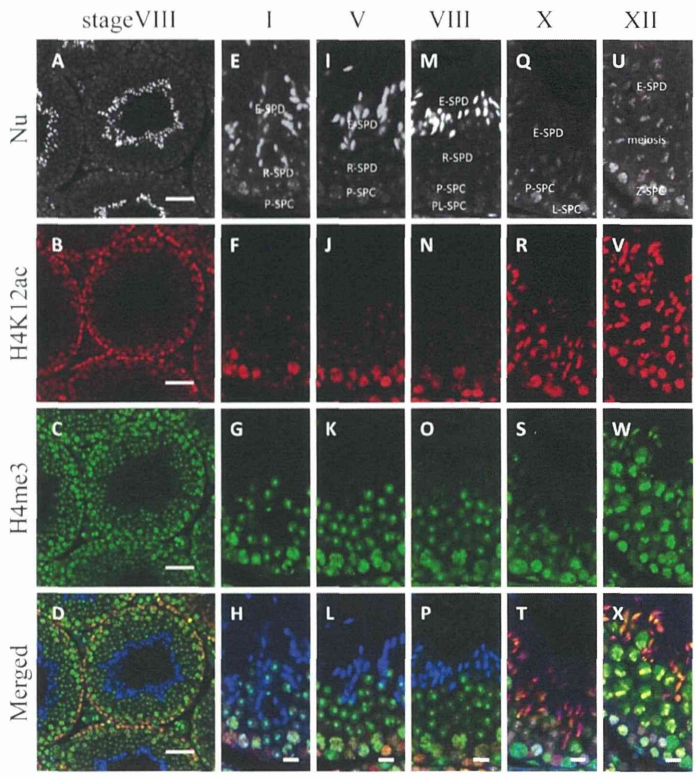

Fig. 2.

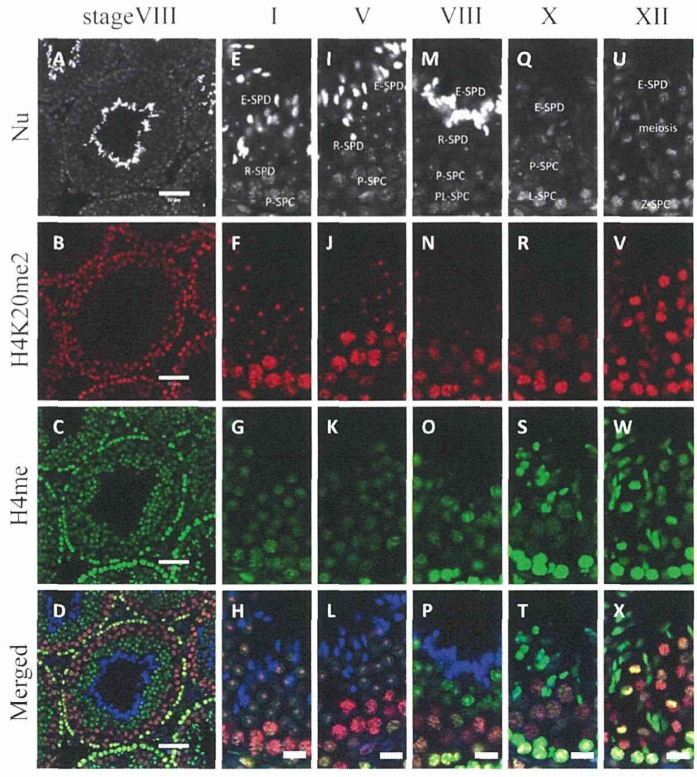

Fig. 3.

Biotechnology), histone H4 lysine 12 acetylation (H4K12ac, sc-8661-R; Santa Cruz Biotechnology) and histone H4 lysine 20 di-methylation (H4K20me2, #9759S; Cell Signaling Technology, Danvers, MA, USA) were used as primary antibodies. Alexa Fluor 488-labeled anti-mouse secondary antibodies (Invitrogen, Life Technologies, Carlsbad, CA, USA) were used against H4me and H4me3. Alexa Fluor 594-labeled donkey anti-rabbit secondary antibodies (Invitrogen) were used against H4K5ac, H4K8ac, H4K12ac and H4K20me2.

Immunohistochemistry

Paraffin-embedded sections (10 μm) were mounted on glass slides. The sections were deparaffinized with xylene, dehydrated with ethanol and subsequently incubated with HistoVT One (Nacalai Tesque, Kyoto, Japan) at 90 C for 30 min to mediate antigen retrieval. The sections were then washed with distilled water, incubated with Blocking One (Nacalai Tesque) at 4 C for 1 h and subsequently incubated with primary antibodies at 4 C overnight [the primary antibodies were added to Blocking One (Nacalai Tesque) and phosphate-buffered saline-mixed liquor (diluted 1:200)]. After incubation, the sections were incubated with Alexa Fluor 488-labeled anti-mouse and Alexa Fluor 594-labeled anti-rabbit secondary antibodies (diluted 1:1000) at 4 C for 3 h. The nuclei were counterstained with Hoechst 33342 (diluted 1:5000; Molecular Probes, Eugene, OR, USA). The stained images were obtained using an LSM-700 confocal laser microscope (Carl Zeiss; Oberkochen, Germany), and the fluorescent brightness was analyzed with the ZEN2010 software in conjunction with the LSM-700 microscope. The stage of each seminiferous tubule was determined following the criteria described previously [24].

Comparison of brightness of fluorescence

We used the ZEN-2010 software in conjunction with the LSM-700 microscope and analyzed the mean of fluorescence intensity in the sperm cells. Fluorescence brightness was classified into 255 levels. We categorized the intensity levels over 200 as "strong," those between 100 and 200 as "moderate," those below 100 as "weak" and those that were extra low as "negative."

Results

Histone H4 lysine 5, 8 and 12 acetylation (H4K5ac, H4K8ac and H4K12ac)

H4K5ac, H4K8ac and H4K12ac showed dynamic changes during the differentiation of male germ cells (Figs. 1 and 2). In spermatogonia, the levels of H4K5ac, H4K8ac and H4K12ac were moderately intense. In preleptotene and leptotene spermatocytes, H4K5ac, H4K8ac and H4K12ac were highly acetylated (Fig. 1H, K, H', K'; Fig. 2N, R). The immunostaining intensity was similar in zygotene spermatocytes (Fig. 1N, N'; Fig. 2V). The expression of H4K5ac, H4K8ac and H4K12ac gradually decreased in pachytene spermatocytes (Fig. 1E–K, E'–K'; Fig. 2F–R). However, H4K5ac, H4K8ac and H4K12ac were highly acetylated during meiosis (Fig. 1N, N'; Fig. 2V). In spermatids, H4K5ac, H4K8ac and H4K12ac were detected in only a portion in step 1–8 spermatids and were highly acetylated in steps 9–12 spermatids (Fig. 1K, N, K', N'; Fig. 2R, V). No acetylation of the histone H4 N-terminal tails was observed in spermatids after step 13.

Histone H4 tri-methylation (H4me3)

H4me3 showed specific exchange during spermatogenesis (Table 1). It showed a weak staining intensity in preleptotene and leptotene spermatocytes (Fig. 2O, S), high intensity staining in zygotene spermatocytes and moderate intensity staining in pachytene spermatocytes (Fig. 2G, K, O, S). High staining intensity was observed during meiosis (Fig. 2W). In the case of round spermatids, a highly modified state was observed in only a portion of the spermatids (Fig. 2G, K, O), and the staining intensity of H4me3 gradually increased in step 9 to 12 spermatids (Fig. 2S, W). However, no stained spermatids were observed after step 13.

Histone H4 lysine 20 di-methylation (H4K20me2)

H4K20me2 varied dynamically during spermatogenesis [25]. Its staining was moderate in spermatogonia, high at the preleptotene spermatocyte stage and similar in leptotene and zygotene spermatocytes (Fig. 3N, R, V). A highly modified state was observed in early pachytene spermatocytes, and this decreased during pachytene stage (Fig. 3F, J, N, R). The expression level of H4K20me2 increased again from diplotene stage to meiotic prophase (Fig. 3V). In round spermatids, H4K20me2 was detected in only a portion of the spermatids and showed a weak intensity by step 9 (Fig. 3F, J, N, R, V). H4K20me2 was not observed in spermatids by step 13.

Histone H4 mono-methylation (H4me)

H4me showed weak expression in spermatogonia. The immunostaining intensity of H4me increased in preleptotene spermatocytes, was similar in leptotene and zygotene spermatocytes (Fig. 3O, S, W), and decreased in pachytene spermatocytes (Fig. 3G, K, O, S). The expression of H4me increased during meiosis (Fig. 3W) and decreased in round spermatids. However, the staining intensity gradually increased in spermatids at around step 8 (Fig. 3O). This state was maintained in spermatids until step 12 but was not observed by step 13.

Fig. 2. Immunohistochemical analysis of H4 tri-methylation and H4 lysine 12 acetylation. The signals represent nuclear (A, E, I, M, Q, U) histone H4 lysine 12 acetylation (H4K12ac) (B, F, J, N, R, V) and histone H4 tri-methylation (H4me3) (C, G, K, O, S, W). Stage VIII seminiferous tubules are shown (A, B, C, D). Stage I (E, F, G, H), stage V (I, J, K, L), stage VIII (M, N, O, P), stage X (Q, R, S, T) and stage XII (U, V, W, X) seminiferous tubules are shown. The scale bars represent 50 μm (A, B, C, D) and 10 μm (H, L, P, T, X). P-SPC, pachytene spermatocyte; PL-SPC, preleptotene spermatocyte; L-SPC, leptotene spermatocyte; Z-SPC, zygotene spermatocyte; R-SPD, round spermatid; and E-SPD, elongated spermatid.

Fig. 3. Immunohistochemical analysis of histone H4 lysine 20 di-methylation and mono-methylation. The signals represent nuclear (A, E, I, M, Q, U) histone H4 lysine 20 di-methylation (H4K20me2) (B, F, J, N, R, V) and histone H4 mono-methylation (H4me) (C, G, K, O, S, W). Stage VIII seminiferous tubule is shown (A, B, C, D). A stage I (E, F, G, H), stage V (I, J, K, L), stage VIII (M, N, O, P), stage X (Q, R, S, T) and stage XII (U, V, W, X) seminiferous tubules are shown. The scale bars represent 50 μm (A, B, C, D) and 10 μm (H, L, P, T, X). P-SPC, pachytene spermatocyte; PL-SPC, preleptotene spermatocyte; L-SPC, leptotene spermatocyte; Z-SPC, zygotene spermatocyte; R-SPD, round spermatid; and E-SPD, elongated spermatid.

Table 1. Modification pattern of histone H4 during mouse spermatogenesis

Spermatogonium	Staining intensity										
	Spermatocyte								Spermatid		
	A+B	PL	L	Z	PI	PVIII	PX	Meiosis	Steps 1–8	Steps 9–12	Steps 13–16
H4K5ac	m	s	s	s	m	m	w	s	w	s	n
H4K8ac	m	s	s	s	m	m	w	s	w	s	n
H4K12ac	m	s	s	s	m	m	w	s	w	s	n
H4me3	m	w	w	s	m	m	m	s	w	m	n
H4K20me2	m	m	s	s	s	m	w	s	w	w	n
H4me	w	s	s	s	w	w	w	s	w m	s	n

PL, preleptotene spermatocyte; L, leptotene spermatocyte; Z, zygotene spermatocyte; PI, pachytene spermatocyte stage I; PVIII, pachytene spermatocyte stage VIII; PX, pachytene spermatocyte stage X; s, strong intensity; m, moderate intensity; w, weak intensity; n, negative

Discussion

In this study, we demonstrated that modification of the histone H4 N-terminal tails undergoes dramatic changes in male germ cells during spermatogenesis. Spermatocyte development consists of the preleptotene, leptotene, zygotene, pachytene and diplotene stages. Each of the spermatocyte stages shows specific patterns of H4 modification. In preleptotene spermatocytes, the expression of H4me, H4K20me2, H4K5ac, H4K8ac and H4K12ac was high, and that of H4me3 was relatively low. The patterns of staining intensity were similar in leptotene and zygotene spermatocytes. DNA and histone proteins are synthesized in the preleptotene stage [26], and histone acetylation is usually associated with transcriptionally active events [7, 8]. Therefore, it is possible that H4 acetylation is involved in these events during this phase. In preleptotene and leptotene spermatocytes, the histone acetylation state was found to be relatively low compared with that in elongating spermatids [27, 28]. However, since we defined strong intensity as an intensity above a certain fluorescence brightness level, our results showed that both spermatocytes and elongating spermatids had strong intensities. The histone H3 acetylation state in spermatocytes is known to be relatively high [19]. Additional investigation of the relationship between histone acetylation and spermatocyte differentiation is necessary.

The expression of H4K5ac, H4K8ac, K4K12ac and H4me decreased in spermatocytes during the pachytene stage, but H4K20me2 and H4me3 were in a highly modified state. However, H4K20me2 decreased in staining intensity until the late pachytene stage, whereas H4me3 remained relatively high during the pachytene stage. The transcriptional activity is thought to be low in pachytene spermatocytes [26, 29, 30], and it may be associated with H4me3.

During meiosis, all the histone H4 N-terminal tails showed relatively high levels of modification. Since the loss of histone methyltransferase in mouse spermatogenesis is inhibited during meiosis [31–33], it is possible that histone modification plays an important role during the meiotic phase. Histone methylation is associated with both transcriptional activation and inactivation, depending on the histone N-terminal residue involved, while acetylation is associated with transcriptional activation [6, 34]. Both methylation and acetylation states exist in meiosis. The conflicting patterns of histone modification observed in many cells such as embryonic stem cells and spermatogonia may be associated with totipotency [19, 35]. Since numerous biological events are involved in male germ cell meiosis, the conflicting histone modification patterns need further examination.

We found moderate modification of only a portion of the spermatids from step 1 to step 8. Only H4me increased in expression from step 1 to step 8. The nuclei were agglutinated gradually in round spermatids, and then gene expression was generally repressed. These results suggest that low levels of H4 acetylation are perhaps associated with the round spermatid state.

The staining intensity of H4K5ac, H4K8ac, H4K12ac and H4me increased in spermatids from steps 9 to 12. However, those of H4K20me2 and H4me3 were maintained in a lower state. In particular, histone H4 acetylation increased dramatically at around step 10 of the spermatid stage. Histone-to -protamine exchange is known to take place during this period [36]. Although little is known about the mechanism of this exchange, histone acetylation is probably associated with this event [28, 37]. Histone acetylation may also contribute to weakening of the binding between DNA and histone and may be involved in histone-to-protamine exchange. Multiple modification patterns depending on mono-, di-, and tri-methylation may also contribute to the histone-to-protamine exchange.

During spermiogenesis, histone proteins are substituted by transition proteins and then subsequently by protamines. However, a small amount of histone proteins is retained in spermatids, and chemical modification of these histones plays an important role in sperm formation [38]. Nevertheless, the retention of histone H4 modifications was not observed in our experiments.

Comparison of the modification patterns of histones H3 and H4 showed that the H3 and H4ac patterns were similar; however, the patterns of H4me3 differed from those of H3K4me3 and H3K27me3. Thus, it is possible that H4me3 and H3 play different roles during murine spermatogenesis [19, 25].

In this study, we used immunohistochemical methods to show that specific patterns of histone H4 modification are present during murine spermatogenesis. These results can provide further insight into the genetic control (e.g., chromatin remodeling, telomere repair, meiosis and histone-to-protamine exchange) of spermatogenesis and shed light on the epigenetic disorders that involve histone H4.

References

1. **Goldberg AD, Allis CD, Bernstein E.** Epigenetics: a landscape takes shape. *Cell* 2007; **128**: 635–638. [Medline] [CrossRef]
2. **Berger SL.** Histone modifications in transcriptional regulation. *Curr Opin Genet Dev* 2002; **12**: 142–148. [Medline] [CrossRef]
3. **Dion MF, Altschuler SJ, Wu LF, Rando OJ.** Genomic characterization reveals a simple histone H4 acetylation code. *Proc Natl Acad Sci USA* 2005; **102**: 5501–5506. [Medline] [CrossRef]
4. **Govin J, Caron C, Lestrat C, Rousseaux S, Khochbin S.** The role of histones in chromatin remodelling during mammalian spermiogenesis. *Eur J Biochem* 2004; **271**: 3459–3469. [Medline] [CrossRef]
5. **Kouzarides T.** Chromatin modifications and their function. *Cell* 2007; **128**: 693–705. [Medline] [CrossRef]
6. **Martin C, Zhang Y.** The diverse functions of histone lysine methylation. *Nat Rev Mol Cell Biol* 2005; **6**: 838–849. [Medline] [CrossRef]
7. **Imhof A, Yang XJ, Ogryzko VV, Nakatani Y, Wolffe AP, Ge H.** Acetylation of general transcription factors by histone acetyltransferases. *Curr Biol* 1997; **7**: 689–692. [Medline] [CrossRef]
8. **Grunstein M.** Histone acetylation in chromatin structure and transcription. *Nature* 1997; **389**: 349–352. [Medline] [CrossRef]
9. **Kuo MH, Allis CD.** Roles of histone acetyltransferases and deacetylases in gene regulation. *BioEssays* 1998; **20**: 615–626. [Medline] [CrossRef]
10. **Trojer P, Reinberg D.** Histone lysine demethylases and their impact on epigenetics. *Cell* 2006; **125**: 213–217. [Medline] [CrossRef]
11. **Endo T, Naito K, Aoki F, Kume S, Tojo H.** Changes in histone modifications during in vitro maturation of porcine oocytes. *Mol Reprod Dev* 2005; **71**: 123–128. [Medline] [CrossRef]
12. **Gu L, Wang Q, Sun QY.** Histone modifications during mammalian oocyte maturation: dynamics, regulation and functions. *Cell Cycle* 2010; **9**: 1942–1950. [Medline] [CrossRef]
13. **Endo T, Imai A, Shimaoka T, Kano K, Naito K.** Histone exchange activity and its correlation with histone acetylation status in porcine oocytes. *Reproduction* 2011; **141**: 397–405. [Medline] [CrossRef]
14. **Franciosi F, Lodde V, Goudet G, Duchamp G, Deleuze S, Douet C, Tessaro I, Luciano AM.** Changes in histone H4 acetylation during in vivo versus in vitro maturation of equine oocytes. *Mol Hum Reprod* 2012; **18**: 243–252. [Medline] [CrossRef]
15. **Seneda MM, Godmann M, Murphy BD, Kimmins S, Bordignon V.** Developmental regulation of histone H3 methylation at lysine 4 in the porcine ovary. *Reproduction* 2008; **135**: 829–838. [Medline] [CrossRef]
16. **Kim JM, Liu H, Tazaki M, Nagata M, Aoki F.** Changes in histone acetylation during mouse oocyte meiosis. *J Cell Biol* 2003; **162**: 37–46. [Medline] [CrossRef]
17. **Khalil AM, Wahlestedt C.** Epigenetic mechanisms of gene regulation during mammalian spermatogenesis. *Epigenetics* 2008; **3**: 21–28. [Medline] [CrossRef]
18. **Teng YN, Kuo PL, Cheng TC, Liao MH.** Histone gene expression profile during spermatogenesis. *Fertil Steril* 2010; **93**: 2447–2449. [Medline] [CrossRef]
19. **Song N, Liu J, An S, Nishino T, Hishikawa Y, Koji T.** Immunohistochemical Analysis of Histone H3 Modifications in Germ Cells during Mouse Spermatogenesis. *Acta Histochem Cytochem* 2011; **44**: 183–190. [Medline] [CrossRef]
20. **Wang H, Huang ZQ, Xia L, Feng Q, Erdjument-Bromage H, Strahl BD, Briggs SD, Allis CD, Wong J, Tempst P, Zhang Y.** Methylation of histone H4 at arginine 3 facilitating transcriptional activation by nuclear hormone receptor. *Science* 2001; **293**: 853–857. [Medline] [CrossRef]
21. **Sanders SL, Portoso M, Mata J, Bähler J, Allshire RC, Kouzarides T.** Methylation of histone H4 lysine 20 controls recruitment of Crb2 to sites of DNA damage. *Cell* 2004; **119**: 603–614. [Medline] [CrossRef]
22. **Shogren-Knaak M, Ishii H, Sun JM, Pazin MJ, Davie JR, Peterson CL.** Histone H4-K16 acetylation controls chromatin structure and protein interactions. *Science* 2006; **311**: 844–847. [Medline] [CrossRef]
23. **Krishnamoorthy T, Chen X, Govin J, Cheung WL, Dorsey J, Schindler K, Winter E, Allis CD, Guacci V, Khochbin S, Fuller MT, Berger SL.** Phosphorylation of histone H4 Ser1 regulates sporulation in yeast and is conserved in fly and mouse spermatogenesis. *Genes Dev* 2006; **20**: 2580–2592. [Medline] [CrossRef]
24. **Russell LD.** Histological and histopathological evaluation of the testis. 1990.
25. **Payne C, Braun RE.** Histone lysine trimethylation exhibits a distinct perinuclear distribution in Plzf-expressing spermatogonia. *Dev Biol* 2006; **293**: 461–472. [Medline] [CrossRef]
26. **Erickson RP.** Post-meiotic gene expression. *Trends Genet* 1990; **6**: 264–269. [Medline] [CrossRef]
27. **Morinière J, Rousseaux S, Steuerwald U, Soler-López M, Curtet S, Vitte AL, Govin J, Gaucher J, Sadoul K, Hart DJ, Krijgsveld J, Khochbin S, Müller CW, Petosa C.** Cooperative binding of two acetylation marks on a histone tail by a single bromodomain. *Nature* 2009; **461**: 664–668. [Medline] [CrossRef]
28. **Hazzouri M, Pivot-Pajot C, Faure AK, Usson Y, Pelletier R, Sèle B, Khochbin S, Rousseaux S.** Regulated hyperacetylation of core histones during mouse spermatogenesis: involvement of histone deacetylases. *Eur J Cell Biol* 2000; **79**: 950–960. [Medline] [CrossRef]
29. **Khalil AM, Boyar FZ, Driscoll DJ.** Dynamic histone modifications mark sex chromosome inactivation and reactivation during mammalian spermatogenesis. *Proc Natl Acad Sci USA* 2004; **101**: 16583–16587. [Medline] [CrossRef]
30. **Turner JM.** Meiotic sex chromosome inactivation. *Development* 2007; **134**: 1823–1831. [Medline] [CrossRef]
31. **Hayashi K, Yoshida K, Matsui Y.** A histone H3 methyltransferase controls epigenetic events required for meiotic prophase. *Nature* 2005; **438**: 374–378. [Medline] [CrossRef]
32. **Peters AH, O'Carroll D, Scherthan H, Mechtler K, Sauer S, Schöfer C, Weipoltshammer K, Pagani M, Lachner M, Kohlmaier A, Opravil S, Doyle M, Sibilia M, Jenuwein T.** Loss of the Suv39h histone methyltransferases impairs mammalian heterochromatin and genome stability. *Cell* 2001; **107**: 323–337. [Medline] [CrossRef]
33. **Tachibana M, Sugimoto K, Nozaki M, Ueda J, Ohta T, Ohki M, Fukuda M, Takeda N, Niida H, Kato H, Shinkai Y.** G9a histone methyltransferase plays a dominant role in euchromatic histone H3 lysine 9 methylation and is essential for early embryogenesis. *Genes Dev* 2002; **16**: 1779–1791. [Medline] [CrossRef]
34. **Schübeler D, MacAlpine DM, Scalzo D, Wirbelauer C, Kooperberg C, van Leeuwen F, Gottschling DE, O'Neill LP, Turner BM, Delrow J, Bell SP, Groudine M.** The histone modification pattern of active genes revealed through genome-wide chromatin analysis of a higher eukaryote. *Genes Dev* 2004; **18**: 1263–1271. [Medline] [CrossRef]
35. **Bernstein E, Duncan EM, Masui O, Gil J, Heard E, Allis CD.** Mouse polycomb proteins bind differentially to methylated histone H3 and RNA and are enriched in facultative heterochromatin. *Mol Cell Biol* 2006; **26**: 2560–2569. [Medline] [CrossRef]
36. **Dada R, Kumar M, Jesudasan R, Fernández JL, Gosálvez J, Agarwal A.** Epigenetics and its role in male infertility. *J Assist Reprod Genet* 2012; **29**: 213–223. [Medline] [CrossRef]
37. **Awe S, Renkawitz-Pohl R.** Histone H4 acetylation is essential to proceed from a histone- to a protamine-based chromatin structure in spermatid nuclei of Drosophila melanogaster. *Syst Biol Reprod Med* 2010; **56**: 44–61. [Medline] [CrossRef]
38. **Hammoud SS, Nix DA, Zhang H, Purwar J, Carrell DT, Cairns BR.** Distinctive chromatin in human sperm packages genes for embryo development. *Nature* 2009; **460**: 473–478. [Medline]

BIOLOGY OF REPRODUCTION (2014) 91(2):53, 1–9
Published online before print 16 July 2014.
DOI 10.1095/biolreprod.113.112789

Neurotensin Enhances Sperm Capacitation and Acrosome Reaction in Mice

Yuuki Hiradate,[1,2] Hiroki Inoue,[2] Norio Kobayashi,[2] Yoshiki Shirakata,[2] Yutaka Suzuki,[4] Aina Gotoh,[6] Sang-gun Roh,[4] Takafumi Uchida,[6] Kazuo Katoh,[4] Manabu Yoshida,[5] Eimei Sato,[3] and Kentaro Tanemura[2]

[2]*Laboratory of Animal Reproduction, Graduate School of Agricultural Science, Tohoku University, Sendai, Japan*
[3]*National Livestock Breeding, Fukushima, Japan*
[4]*Laboratory of Animal Physiology, Graduate School of Agricultural Science, Tohoku University, Sendai, Japan*
[5]*Misaki Marine Biological Station, Graduate School of Science, University of Tokyo, Kanagawa, Japan*
[6]*Laboratory of Enzymology, Graduate School of Agricultural Science, Tohoku University, Sendai, Japan*

ABSTRACT

Neurotensin (NT) has multiple functions, ranging from acting as a neurotransmitter to regulating intestinal movement. However, its function in reproductive physiology is unknown. Here, we confirmed the expression and localization of NT receptors (NTR1) in mouse epididymal spermatozoa and investigated the effect of NT on sperm function. Sperm protein tyrosine phosphorylation, one of the indices of sperm capacitation, was facilitated dose-dependently by NT administration. In addition, the acrosome reaction was promoted in capacitated spermatozoa, and addition of a selective antagonist of NTR1 and NTR2 blocked the induction. Furthermore, intracellular calcium mobilization by NT addition was observed. This showed that NT was an accelerator of sperm function via its functional receptors. The presence of NT was confirmed by immunohistochemistry and its localization was observed in epithelia of the uterus and oviduct isthmus and ampulla, which correspond to the fertilization route of spermatozoa. The NT mRNA level in ovulated cumulus cell was remarkably increased by treatment with human chorionic gonadotropin (hCG). Using an in vitro maturation model, we analyzed the effects of FSH, epidermal growth factor (EGF), estradiol, and progesterone in NT production in cumulus cells. We found that FSH and EGF upregulated NT release and mRNA expression. Both FSH- and EGF-induced upregulation were inhibited by U0126, an MAPK kinase inhibitor, indicating that FSH and EGF regulate NT expression via a MAPK-dependent pathway. This evidence suggests that NT can act as a promoter of sperm capacitation and the acrosome reaction in the female reproductive tract.

acrosome reaction, capacitation, cumulus cells, fertilization, oviduct, ovulation, reproduction, sperm, uterus

INTRODUCTION

Mammalian spermatozoa are infertile when immediately ejaculated and need to acquire fertilizing ability by capacitation when passing through the female reproductive tract toward the oviductal ampulla, the region of fertilization [1]. Only a limited number of spermatozoa reaching the ampulla undergo acrosomal exocytosis (the acrosome reaction) and are able to fertilize. During this journey, spermatozoa are exposed to various factors that regulate sperm function, including some that facilitate or inhibit capacitation and the acrosome reaction. Ions and proteins, ranging from bicarbonate to albumin, activate the cAMP production and protein kinase A (PKA) pathway and accelerate tyrosine phosphorylation or remove cholesterol from the sperm plasma membrane [2, 3]. Numerous factors secreted from the female reproductive tissues are involved in this complex process.

Several reports have provided evidence of some neurotransmitter receptors in sperm, which had been considered to work in central nervous systems, such as gamma aminobutyric acid [4], dopamine [5], or serotonin [6]. These receptors are stimulated by the corresponding ligand and regulate sperm capacitation or the acrosome reaction.

Neurotensin (NT), which consists of 13 amino acids excised from an NT precursor, is a hormone first isolated from the bovine hypothalamus as a hypotensive peptide [7]. In the brain, its function is as a modulator of the dopaminergic system [8, 9]. However, it is not only found in the central nervous system, but also in the small intestine and stomach [10] where it participates in gastrointestinal motility and secretion [11]. Furthermore, the NT receptor is present in lymphocytes [12]. These reports suggest multiple functions for NT.

Several studies have shown that NT has three types of receptors (NTRs), named NTR1, NTR2, and NTR3 [13]. NTR1 and NTR2 belong to a family of receptors with seven transmembrane spanning domains and are coupled to G proteins (G protein-coupled receptors), whereas NTR3 belongs to the family of sorting receptors [14]. Early studies reported that most of the biological changes induced by NT act via NTR1 or NTR2 [15–17]; for example, in gastrointestinal motility [18] or in glutamate signaling in the brain [19].

Although the interactions between NT and its receptors in several cell types have been investigated, there is limited information regarding their functions in reproductive physiology. It is well-known that female reproductive organs and cumulus cells secrete factors affecting sperm fertilizing competence [20–22]. Because NT stimulation produces second messengers, such as cAMP or $Ca2^{+}$, these are essential for acquisition of sperm fertility functions. We here aimed to clarify how NT effects sperm functions. In addition, NT expression patterns were analyzed in female reproductive organs and cumulus cells to elucidate how NT expression might be controlled.

[1]Correspondence: Yuuki Hiradate, Laboratory of Animal Reproduction, Graduate School of Agricultural Science, Tohoku University, Aoba-ku, Sendai 981-8555, Japan. E-mail: hiradate@bios.tohoku.ac.jp

Received: 1 August 2013.
First decision: 3 September 2013.
Accepted: 17 June 2014.

eISSN: 1529-7268 http://www.biolreprod.org
ISSN: 0006-3363

MATERIALS AND METHODS

Ethics

All the experimental procedures involving animals were conducted in accordance with the Society for the Study of Reproduction's guidelines and standards.

Chemicals

All the chemicals were purchased from Sigma (Sigma-Aldrich Japan Ltd.) unless otherwise stated.

Mouse Sperm Preparation

BL57BL/6 mice were purchased from Japan SLC, Inc. Cauda epididymal sperm were collected from male mice (aged >12 wk), which were euthanized in accordance with the Guide for the Care and Use of Laboratory Animals published by Tohoku University. Epididymis from each animal was placed in 500 µl of human tubal fluid (HTF) medium [23], consisting of 101.6 mM NaCl, 4.7 mM KCl, 0.37 mM K_2PO_4, 0.2 mM $MgSO_4 \cdot 7H_2O$, 2 mM $CaCl_2$, 25 mM $NaHCO_3$, 2.78 mM glucose, 0.33 mM pyruvate, 21.4 mM sodium lactate, 286 mg/L penicillin G, 228 mg/L streptomycin, and 5 mg/ml of fatty acid-free bovine serum albumin (BSA). The medium containing sperm cells was covered with sterile paraffin oil (Nacalai Tesque, Inc.) at 37°C for 90 min for capacitation under 5% CO_2 in humidified air. After 10 min of diffusion, the sperm concentration was adjusted as desired and used for the following experiments. All the experiments were performed using pooled semen samples from at least three mice.

Isolation of Cumulus-Oocyte Complexes for In Vitro Maturation

The 4-wk-old immature female mice were stimulated with 5 international units (IU) of equine chorionic gonadotropin (eCG) (Asuka Pharmaceuticals) for 48 h. Cumulus-oocyte complexes (COCs) were collected from large antral follicles punctured with 26-gauge needles in Leibovitz L-15 medium (Invitrogen) containing 0.1% polyvinyl alcohol. Collected COCs were used for in vitro maturation (IVM). The COCs were cultured in Waymouth MB 752/1 medium (Invitrogen) supplemented with 1% fetal calf serum (Sankyo Kagaku), 0.23 mM pyruvic acid (Nacalai Tesque, Inc.), 75 mg/L penicillin G (Meiji Seika), and 50 mg/L streptomycin sulfate (Meiji Seika) at 37°C under humidified 5% CO_2 in air.

Indirect Immunofluorescence Analysis of Sperm

Indirect immunofluorescence analysis was performed to investigate the localization of NTR1 and NTR2 in spermatozoa. Epididymal sperm were suspended in HTF medium and collected by centrifugation at 1000 × *g* for 5 min and fixed with 2% paraformaldehyde in PBS for 15 min at 4°C. They were then washed twice with 1% BSA in PBS, permeabilized with 1% Triton X in PBS for 10 min at room temperature, and blocked with Blocking One (Nacalai Tesque, Inc.) for 60 min at 4°C. The suspensions were incubated with mouse monoclonal anti-NTR1 (sc-374492, 1:100; Santa Cruz Biotechnology) antibody overnight at 4°C. After being washed three times with 1% BSA in PBS, suspensions were incubated for 60 min at room temperature with anti-rabbit immunoglobulin M-Alexa Fluor 488 (1:500; Molecular Probes Life Technologies Corp.) for 60 min at room temperature. Finally, treated samples were washed, suspended in 1% BSA in PBS, mounted on glass slides, and covered with glass. As the negative control for NTR1 immunoreaction, the primary antibody was preincubated with a 10-fold molar excess of the synthetic peptide (Genscriptjapan) for 1 h, and preabsorbed antibody was used for the immunofluorescent analysis.

Immunohistochemical Staining of Oviduct and Uterus

Mice primed with 5 IU eCG for 48 h and then with 5 IU of human chorionic gonadotropin (hCG) were euthanized after 14 h. Ovary-attached oviduct from four or five mice were dissected after cervical dislocation and immersed in Bouin fixing solution for 4 h at room temperature. Fixed tissues were embedded in paraffin, cut to 5 µm, and mounted on glass slides. After deparaffinization and rehydration, antigen was retrieved by immersion in HistoVT (Nacalai Tesque, Inc.) for 30 min at 90°C. The slides were then blocked with 1% BSA-PBS for 60 min at 4°C and incubated overnight at 4°C with a rabbit polyclonal primary antibody against NT (ab43833, 1:100; Abcam). The primary antibody was also preincubated with a 10-fold molar excess of antigen-blocking peptide for 1 h at room temperature. This preabsorbed antibody was used as the negative control. After washing in PBS for 10 min, the slides were incubated with a second antibody against anti-rabbit immunoglobulin G-Alexa Fluor 488 diluted 1:1000 with PBS and propidium iodide diluted 1:10 000 for 60 min at room temperature. After washing with PBS, slides were covered with glass. Stained tissues were visualized using a confocal laser scanning fluorescence microscope (LSM700; Zeiss).

Western Blot Analysis

Detection of NTR1 in sperm extraction. Spermatozoa suspended in HTF medium were collected by centrifugation. RIPA buffer (50 mM Tris-HCl, pH 7.6, 150 mM NaCl, 1% Nonidet P40, 0.5% sodium deoxycholate, and 1% protease inhibitor) (Nacalai Tesque) was added to the sperm pellet and sonicated to extract the proteins. The sample was boiled for 5 min, centrifuged, and the supernatants were used. The protein concentration in the supernatants was determined using the bicinochoninic acid protein assay kit (Thermo Scientific). The same volume of 2× Laemmli sample buffer was added to the extracted solutions for reducing. The proteins were separated by SDS-PAGE and transferred to polyvinylidene difluoride membranes. Membrane blocking was performed for 60 min at room temperature. After three washes with PBS containing 0.1% Tween 20, the proteins were treated with primary antibodies (anti-NTR1; 1:4000) overnight at 4°C, then washed three times with PBS containing 0.1% Tween 20. The proteins were treated with horseradish peroxidase (HRP)-conjugated anti-mouse immunoglobulin M antibody (1:2000; Santa Cruz Biotechnology) for 1 h at room temperature. After two washes, the membrane was reacted with Chemilumi One (Nacalai Tesque), and images were obtained using an LAS-3000-mini Lumino Image Analyzer (Fujifilm).

Tyrosine phosphorylation. To detect sperm protein tyrosine phosphorylation, the sperm concentration was adjusted to 5×10^6/ml in each treatment group and equivalent volumes of suspension were divided into microtubes. Saline (control) and NT (Calbiochem) dissolved in saline were added at determined final concentrations, and the suspensions were cultured for 60 min under 5% CO_2 in air at 37°C. After incubation, a sperm pellet was obtained by centrifugation at 8000 × *g* for 5 min; the proteins were extracted and reduced as described above, subjected to 10% SDS-PAGE, and transferred. After 60 min of blocking, samples were treated with a mouse monoclonal anti-phosphotyrosine 4G10 antibody (05–321, 1:10 000; Upstate Cell Signaling Solutions) or anti-α-tubulin (T9026, 1:5000; Sigma-Aldrich) overnight at 4°C. After three washes, the membrane was treated with an HRP-conjugated anti-mouse antibody for 60 min at room temperature, and images were obtained as described above.

Effects of NT on the Acrosome Reaction

Spermatozoa were capacitated in HTF medium for 90 min. After equal volumes of the suspension were divided into microtubules (5×10^6), NT stock solution or antagonist of NTR1 and NTR2 was added to each suspension at the desired concentration. After 30 min incubation at 37°C, the suspensions were smeared onto glass slides and air-dried. Evaluation of acrosome reactions was assessed by staining with fluorescein isothiocyanate-conjugated peanut agglutinin lectin (J Oil Mills) diluted 1:100 in a light-shielded humidity chamber for 30 min. Slides were washed several times with PBS and covered. The number of spermatozoa with which acrosome reacted was determined under a fluorescence microscope. Duplicate counting of at least 200 spermatozoa was performed. The acrosome reaction rate was evaluated by calculating the number of acrosome reacted sperm cells per total counted.

Measurements of NT Induced Intracellular Ca^{2+} Mobilization in Single Sperm

Measurement of intracellular Ca^{2+} ($[Ca^{2+}]_i$) mobilization in single sperm was performed as described previously [24] with some modifications. Briefly, capacitated cauda epididymal sperm were loaded with 4 µM fluo4-AM (Dojindo) for 10 min at 37°C and immobilized on a laminin-coated glass-bottom dish. Observation was performed using inverted microscope (IX-70; Olympus) through a 60× objective (n.a. 1.4; Olympus) with a digital CCD camera (ORCA-ERG; Hamamatsu Photonics). On-line control of the system, acquisition, and off-line analysis of the collected data were done with TI Workbench software (written by T. Inoue) running on a Macintosh computer. Levels of $[Ca2+]_i$ are calculated as F/F0 ratios after background subtraction in both images and time-course plots. The experiments were performed with a heating chamber covering the stage and objective lens of the microscope.

Quantitative Analysis of NT mRNA in Female Reproductive Tissues and Cumulus Cells by RT-PCR Total RNA Extraction

Total RNA was obtained from tissue dissected from mice primed with 5 IU of eCG for 48 h following hCG for 14 h. The uterine horns and oviducts were separated, and the oviductal isthmus and ampulla were dissected apart, frozen immediately in liquid nitrogen and kept at −80°C until RNA extraction. RNA extraction was performed using ISOGEN (Nippon Gene).

For comparisons between cumulus cells from immature COCs and superovulated COCs, the former were collected from immature female mice. Cumulus cells from superovulated mice treated with eCG and then hCG were collected from dissected oviductal ampullae at 14 h after hCG treatment. Cumulus cells were removed from the COCs with a glass pipette and transferred into a microtube, washed twice in PBS, and centrifuged for collection. Total RNA expression was performed using RNeasy micro kits (Qiagen) following the manufacturer's instructions.

Quantitative RT-PCR

Total RNA from tissues or cumulus cells was reverse transcribed and cDNA synthesized using Rever Tra Ace (Nacalai Tesque). Specific primers were designed on the basis of the sequences of NT (forward: CCTGACTCTCCTGGC; reverse: TTTCCAAGACGGAGGACTTGC) and *18S* (forward: GGGGAATCAGGGTTCGAT; reverse: GGCCTCGAAA GAGTCCTGTA) as an internal control. The program consisted of 44 cycles of denaturation at 94°C for 5 sec, annealing at 61°C for 20 sec, and extension at 72°C for 15 sec, with an additional extension at 72°C for 5 min. To confirm whether the correct gene was amplified, the obtained products were loaded onto 2% agarose gels and electrophoresed. The NT mRNA expression levels were normalized to the *18S* mRNA level. The mean sample and endogenous control threshold cycles (Ct) for each sample were calculated using the ($2^{-\Delta\Delta Ct}$) method.

Measurement of NT Concentration

Fifty COCs were cultured in 50-μl aliquots of HTF medium supplemented with FSH (0.1 IU/ml), EGF (50 ng/ml), estradiol (E2) (100 nM), or progesterone (P4) (100 nM) using 96-well plates (Nunc MaxiSorp; Thermo Fisher Scientific) for 24 h; 0.1% dimethyl sulfoxide (DMSO) was used as a solvent control. Culture media and COCs were centrifuged at 8000 × *g* for 5 min at 4°C, and the supernatants were collected. The samples were frozen in liquid nitrogen and kept at −80°C until use. The secretion level of NT was determined by enzyme immunoassay (EIA) kits (Phoenix Pharmaceuticals) following the manual's instructions. Briefly, collected media and the standard sample were cultured in each well with primary antibody and biotinylated peptide at room temperature for 2 h. After washing, streptavidin-HRP solution was added and incubated for 1 h. Detection was performed by adding 3,3′,5,5′-tetramethylbenzidine substrate solution at room temperature for 1 h, the absorbance was read at 450 nm, and the results were calculated.

Statistical Analysis

Each experiment was repeated at least three times. Data were analyzed by one-way ANOVA followed by the Bonferroni-Dunn test using STATVIEW (Version 5.0, SAS Institute Inc.). Student *t*-test was applied when means were compared between two groups; $P < 0.05$ was considered significant. Data are represented as the mean ± SD.

RESULTS

Expression of NTR1 in Spermatozoa

Western blot analysis and immunostaining were performed to determine the expression and localization of NTR1 in spermatozoa. As shown in Figure 1, the immunoreactivity of NTR1 was spotlike and observed in all spermatozoa and was abolished by incubating with primary antibody preabsorbed to the peptide synthesized according to the corresponding immunogenic sequences. Western blot analysis revealed that a specific band was detected around 48 kDa, which coincided with the molecular size of NTR1.

Effects of NT on Sperm Protein Tyrosine Phosphorylation and Acrosome Reaction

To demonstrate whether NT affected sperm protein tyrosine phosphorylation, spermatozoa were cultured without or with NT at various concentrations and analyzed using antibodies by Western blots. As shown in Figure 2, sperm protein tyrosine phosphorylation was increased in a concentration-dependent manner by the addition of NT for 60 min of incubation and some tyrosine-phosphorylated protein bands were detected. The detected protein around 110 kDa was not attributed to capacitation [2, 25]. Tyrosine phosphorylated proteins due to capacitation were detected at 32, 35, 42, 45, 50, 60, ~75, 80, 100, and 130 kDa. Herein NT-enhanced phosphotyrosine proteins were at 32, 35, 42, 50, 60 ~75, and 130 kDa. Although phosphorylation of proteins at 80 and 100 kDa were attributed to capacitation, NT did not enhance noted tyrosine phosphorylation.

We also evaluated the effect of NT on the acrosome reaction after 90 min incubation in BSA-containing HTF medium because this reaction was detected after capacitation. Spermatozoa were capacitated and further cultured in the presence of various doses of NT. This treatment significantly accelerated the acrosome reaction in a dose-dependent manner (Fig. 3A). When SR48692 and levocabastine, the specific antagonists of NTR1 and NTR2 [26, 27], respectively, were added, NT-induced acrosome reaction was blocked, suggesting the functional expression of not only NTR1, but also of NTR2 on sperm cells and the contribution of these receptors to acrosome reaction (Fig. 3B).

Measurement of Effect of NT Addition on Single Sperm $[Ca^{2+}]_i$ Level

When 10 or 50 μM NT was added, $[Ca^{2+}]_i$ levels were increased just after addition (Fig. 4). Calcium intensity when 50 μM of NT was added was higher than that of 10 μM, providing evidence for dose dependency in the $[Ca^{2+}]_i$ response. However, the number of sperm cells that immediately increased their calcium levels were low at 50 μM (10 spermatozoa per 29 total examined) and 10 μM (3 spermatozoa per 50 total examined), whereas almost all the sperm experienced increased calcium mobilization when ionomycin was added (24 spermatozoa per 25 total examined).

Comparison of NT mRNA Expression Levels in Female Reproductive Tissues and Cumulus Cells

Ejaculated spermatozoa undergo capacitation when passing through the uterus and oviduct. Therefore, we analyzed NT mRNA levels in the uterus and oviductal isthmus and ampulla of mice primed with eCG followed by hCG. The expression level in the ampulla was significantly higher than in the isthmus or uterus (Fig. 5).

NT Expression Analysis in the Uterus and Oviduct by Immunohistochemistry

Immunohistochemistry analysis using antibody against NT was performed to examine its expression in the uterus and oviduct. NT immunoreactivity was detected in luminal epithelial cells of uterus and oviductal isthmus and ampulla (Fig. 6), but not in smooth muscle cells. These reactivity was observed throughout the epithelial cells, suggesting that this was the source of the NT secretion. In the uterus, immunoreactivity was also detected in the epithelial cells. Negative

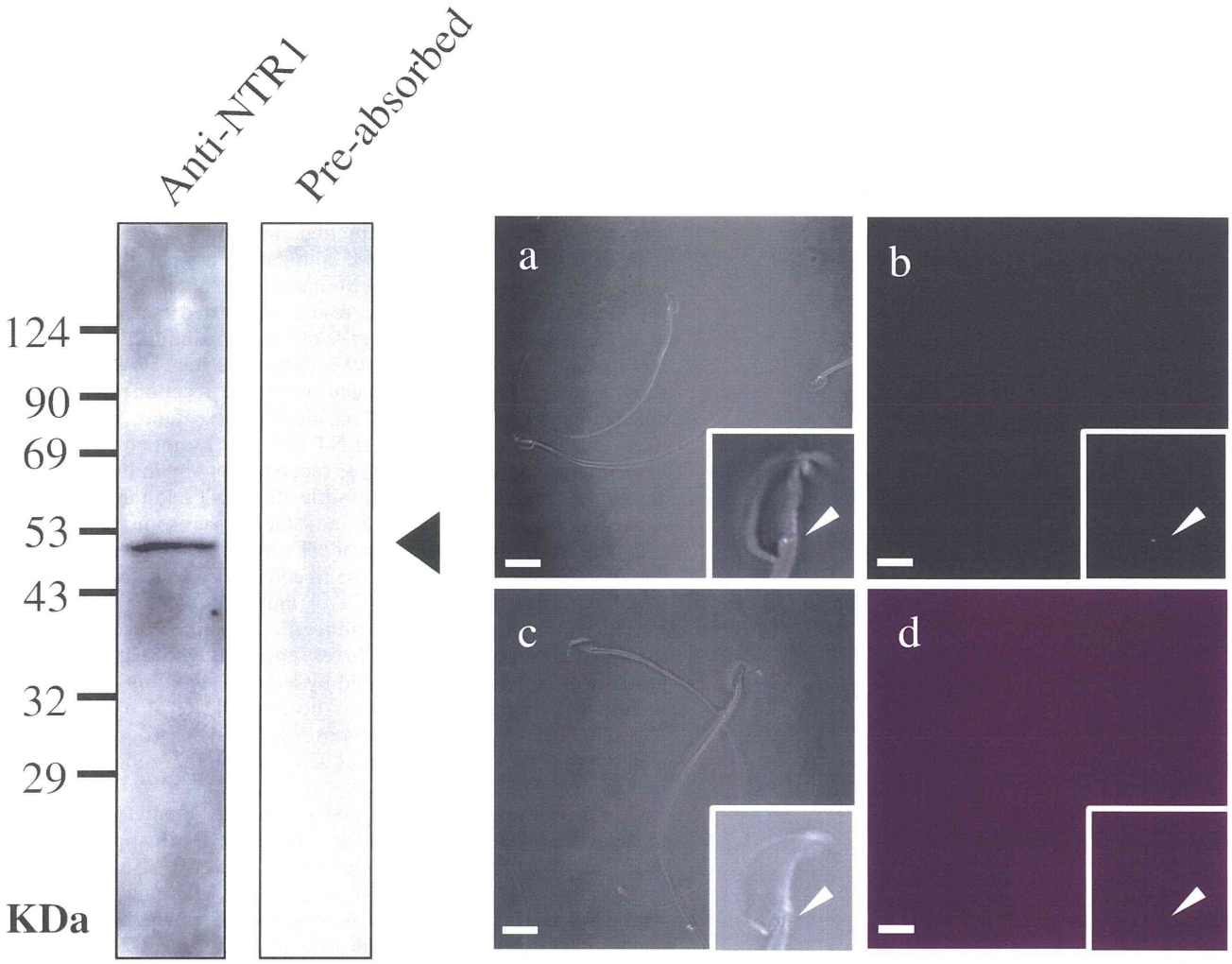

FIG. 1. Detection of NTR1 expression in spermatozoa. NTR1 expression was analyzed by Western blot analysis and immunocytochemistry. Protein extracts from spermatozoa (30 μg) were separated by 10% SDS-PAGE following treatment with specific antibodies. Note the specific band corresponding to NTR1 at the predicted size. The band was not detected when the antibody was incubated with the antigen peptide. Immunofluorescence detection of NTR1 (**a**, **b**). Negative control (preabsorbed antibody; **c**, **d**). Note an immunoreativelike spot was detected at the neck region but was abolished by the absorption test (arrow heads). Bars = 10 μm.

sections incubated with NT antibody with epitope-blocking peptide exhibited no positive staining, and Western blots detected the weaker corresponding bands (Supplemental Fig. S1; available online at www.biolreprod.org).

Effects of Reproductive Hormones on NT Release and NT mRNA Levels in COC Subjected to IVM

The expression of mRNA in superovulated cumulus cells was higher than that in immature, non-eCG treated COCs (Fig. 7A). To determine which reproductive hormone(s) might regulate NT release in cumulus cells, we performed EIA for NT release using an IVM system. COCs collected from eCG-primed mice were cultured in the presence of FSH, EGF, E2, and P4. Addition of FSH or EGF significantly stimulated NT release from cumulus cells after 24 h culture (Fig. 7B). These changes corresponded with the increase in NT mRNA levels (Fig. 7C). When COCs were cultured with FSH or EGF in the presence of U0126, both FSH- and EGF-induced NT mRNA upregulation levels were blocked significantly (Fig. 8).

DISCUSSION

In this study, we investigated the presence of NTR1 in sperm using Western blot analysis and immunocytochemistry (Fig. 1), confirming its expression, and we showed that NT administration in vitro enhanced tyrosine phosphorylation in spermatozoa in a dose-dependent manner (Fig. 2). Visconti et al. [25] showed that tyrosine phosphorylation of several proteins was induced during capacitation. We also detected several tyrosine-phosphorylated proteins, supporting the hypothesis that NT facilitates sperm capacitation.

Sperm protein tyrosine phosphorylation is induced following the elevation of intracytoplasmic cAMP levels following PKA activation [2, 28]. Both NTR1 and NTR2 are coupled with G proteins and interact with the Gs, Gi, or Gq types [14]. Ligand binding on Gs or Gi type-coupled receptors modulate adenylate cyclase activity, regulating cAMP concentration, whereas the Gq type produces inositol-1,4,5-triphosphate and induces Ca^{2+} mobilization.

We also showed that the acrosome reaction in capacitated sperm was dose-dependently facilitated by NT administration and that the pharmacological effects were blocked by either NTR1- or NTR2-specific antagonist (Fig. 3). However,

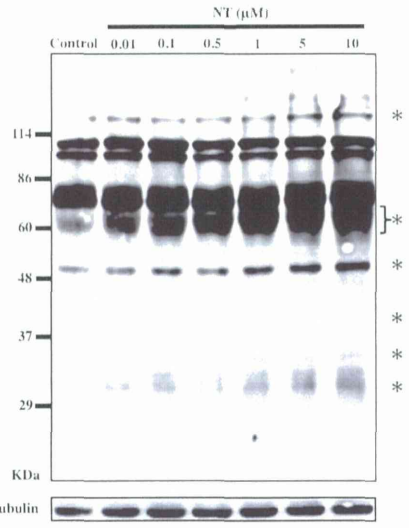

FIG. 2. Effect of NT on sperm protein tyrosine phosphorylation. Mouse epididymal spermatozoa were incubated in the presence of various doses of NT for 60 min. The extracted sperm proteins were separated by 10% SDS-PAGE following treatment with an anti-phosphotyrosine antibody (1:10 000) or anti-α tubulin (1:5000). The protein at 110 kDa was not attributed to capacitation. Note that several dose-dependent increases of tyrosine-phosphorylated bands by NT addition (asterisks) can be seen. The image is representative of at least five repeated experiments with independent sample preparations.

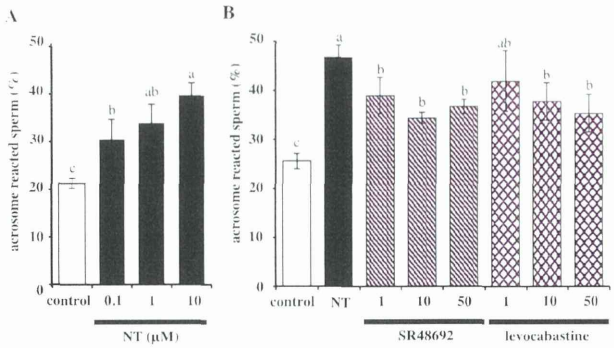

FIG. 3. Effect of NT on the acrosome reaction. Spermatozoa were treated with NT and antagonists. **A**) NT administration enhances acrosome reaction. Mouse spermatozoa were capacitated in HTF medium for 90 min. Saline or various doses of NT (0.1, 1, 10 μM) dissolved in saline was added to equivalent aliquots of the suspension (400 μl aliquots of 5×10^6 sperm/ml) and cultured for 30 min. **B**) Effect of the specific antagonists on NTR1 and NTR2. Antagonists of NTR1 and NTR2 (1, 10, and 50 μM of SR48692 or levocabastine, respectively) were dissolved in DMSO and cultured with sperm suspension in the presence of saline or NT (10 μM). All the groups contained 0.1% DMSO. Examination of the rate of acrosome-reacted spermatozoa was performed using fluorescein isothiocyanate-conjugated peanut agglutinin lectin staining. Each experiment was replicated four times. Data were analyzed by one-way ANOVA followed by Bonferroni-Dunn test. Bars with different letters are significantly different ($P < 0.05$; $n = 4$). Data are shown as the mean ± SD.

complete blocking of acrosome reaction was not observed when each inhibitor was added even at concentration as high as 50 μM; this is possibly due to unaffected receptor functioning in the presence of either inhibitor. Another possibility is contribution by NTR3. NTR3 is not a G protein-coupled receptor and is identical to sortilin [29]. It is not clear whether NTR3, unlike NTR1 and NTR2, mediates second messenger production. Although it has been reported that NTR3 is mainly located intracellularly [30], another study suggested its localization in cell surface in transfected COS-7 cells [31]. The function of NTR3 on sperm cells should be determined when the appropriate specific chemicals are established.

The acrosome reaction is an exocytotic process triggered by an elevation of $[Ca^{2+}]_i$ levels [32, 33]. NTR1 stimulation results in an elevation of Ca^{2+} in human corneal keratinocytes, also suggesting a coupling with Gq-type G proteins [34]. However, there are currently no experimental data showing that Ca^{2+} mobilization is induced by NT stimulation in sperm cells. In order to demonstrate that, calcium imaging in single sperm cells was performed (Fig. 4). These results suggested that although there are certainly some sperm cells that directly induced calcium mobilization by NT addition, the number was few. However, as shown in Figure 3, NT-enhanced acrosome reaction rate was dose-dependently increased. Considering these facts, it seems likely that major contribution of NT on sperm is not attributable to the immediate stimulation of its receptors, but by inducing the acrosome reaction, it is possible that NT enhances the capacitation, and the resulting spontaneous acrosome reaction was induced during the 30 min of NT exposure. In other words, the main function of NT could be to enhance capacitation rather than have an effect on direct $[Ca^{2+}]_i$ mobilization.

Thus, whether the NT-induced acrosome reaction is regulated directly by Ca^{2+} fluxes coupled with Gq-type G proteins or is indirectly mediated by another signaling pathway is still to be determined. This is because NTRs also activate phospholipase C, which produces inositol-1,4,5-triphosphate and triggers the mobilization of Ca^{2+} from the endoplasmic reticulum [35].

It is hypothesized that NT and its receptor-mediated signal transduction system contribute to important fertility phenomena locally at the sites where NT is secreted. Hence, we investigated the localization of NT in the uterus and oviduct, which are important points in the route of spermatozoa during the fertilization process. In the present study, the NT mRNA level, not the protein level of the tissues, was compared to prevent interfusion from other tissues. The NT mRNA level in oviduct ampulla was significantly higher than that in the isthmus and uterus (Fig. 5). Immunoreactivity against NT was detected in endometrium epithelium of the uterus and epithelial cells of oviductal isthmus and ampulla, suggesting NT secretion (Fig. 6). It is well-known that several factors secreted from the uterus and oviduct epithelial cells facilitate capacitation and the acrosome reaction [36–38]. Our results provide the first evidence that NT is one of the factors that facilitate sperm functions. Interestingly, we also found that when NT mRNA levels in cumulus cells were compared between immature COCs and hCG-induced ovulated COCs, the mRNA level in ovulated cumulus cells was markedly higher (Fig. 7A). It has been reported that cumulus cells secrete several acrosome reaction-enhancing factors, such as progesterone [39, 40]. These results suggest the possibility that NT secreted from cumulus cells is one of the enhancers of acrosome reaction. Also, NT might act as a paracrine messenger, and secretion is upregulated by gonadotropin treatment in vivo.

To clarify the factor responsible for upregulation of NT secretion in cumulus cells, we evaluated the amount of released NT from cumulus cells in the presence of FSH, EGF, E2, or P4 in an IVM system. EGF-like factors are mainly released from granulosa cells in response to the LH surge, which facilitates oocyte maturation via the EGF receptor pathway [41], and FSH also stimulates oocyte meiotic resumption through the FSH receptor pathway. Additionally, hCG treatment increases the levels of E2 and P4 in serum [42]. Addition of both FSH and EGF significantly stimulated NT release from cumulus cells;

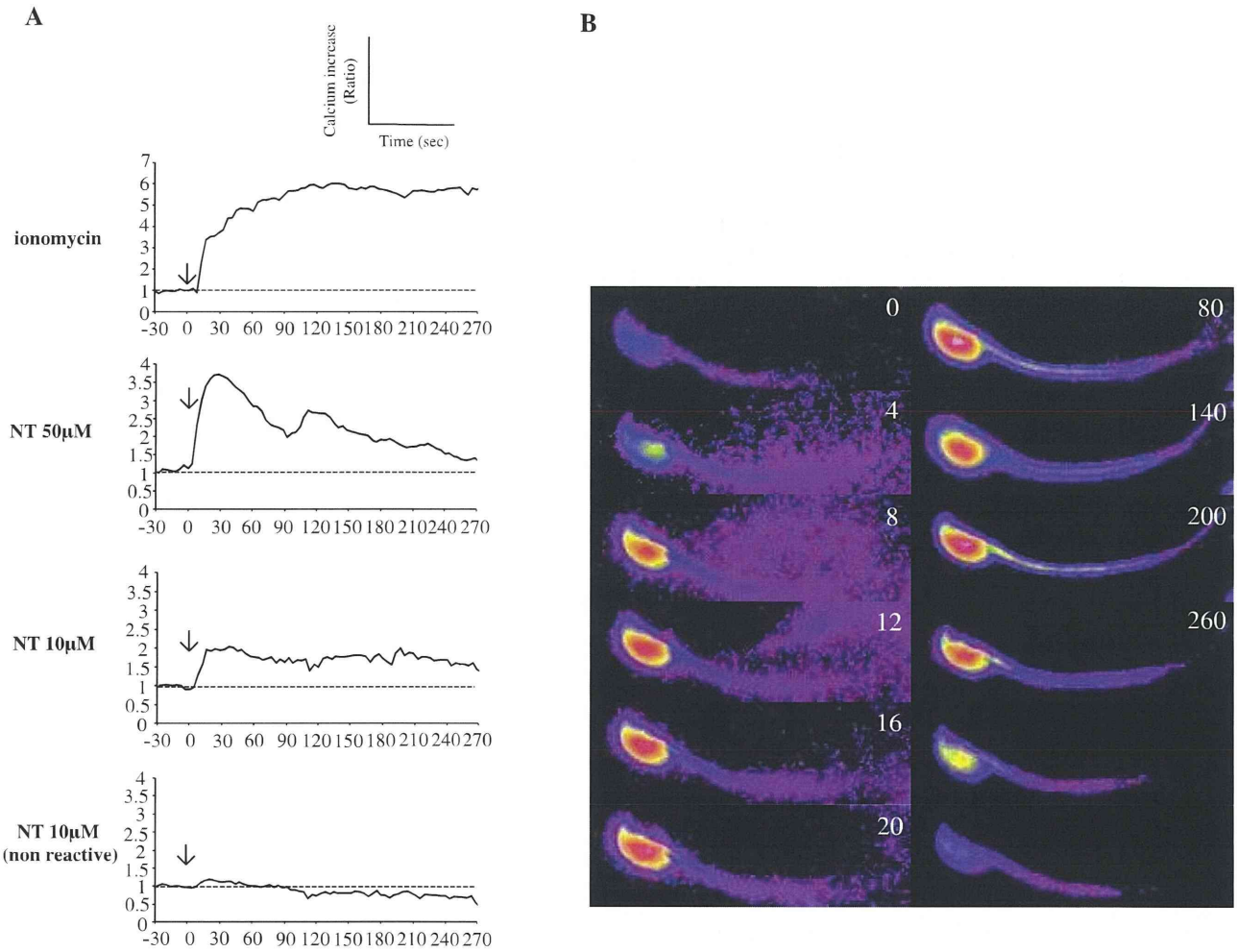

FIG. 4. NT induced sperm $[Ca^{2+}]_i$ mobilization. Capacitated sperm were loaded with 4 μM fluo4-AM for 10 min, and Ca^{2+} responses were monitored every 4 sec. **A**) Intracellular Ca^{2+} levels are expressed as F/F0 ratios. Sperm were treated with ionomycin (2 μM) as a positive control or NT (10 or 50 μM). **B**) Changes in $[Ca^{2+}]_i$ in sperm head area. Representative Ca^{2+} patterns induced by the ligand are used here. Independent experiments were repeated at least five times. The numbers represent seconds. See Supplemental Movie S1.

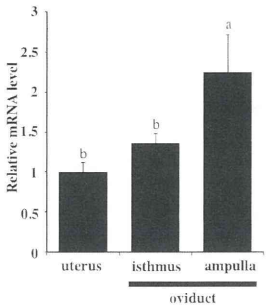

FIG. 5. Comparison of NT mRNA expression levels in female reproductive tissues. The mRNA expression levels of NT in the uterus and oviduct (isthmus and ampulla) were measured using quantitative RT-PCR. The tissues from three or four mice were collected in each experiment. Each experiment was replicated three times. Mice were primed with eCG for 48 h and with hCG 14 h before collecting tissues. The mRNA expression level in the uterus was normalized to 1.0. Data are shown as the mean ± SD ($P < 0.05$; n = 3).

moreover, NT mRNA expression was upregulated by EGF and FSH (Fig. 7, B and C). These results are the first evidence to show that NT expression in cumulus cells is regulated by FSH and EGF.

The highest amounts of NT were measured when COCs were cultured with FSH at 20.16 ± 2.78 pg/50 COCs. Based on a molecular weight of NT of 1673, 8.365 pg/50 COCs = 100 nM, a concentration that has a significant effect on sperm functions in our in vitro experimental system. However, considering the evidence of the remarkable difference in NT mRNA levels between immature and ovulated COCs, we can presume that numerous paracrine factors from cumulus cells or oviducts in vivo further amplified the secretion level. Several studies have suggested that ejaculated spermatozoa are attached to a sperm reservoir and that these attached spermatozoa reach the ampulla and make contact with the COCs to induce the acrosome reaction [43]. Thus, NT-secreted levels from not only cumulus cells but also from oviduct ampulla should be taken into account when considering effective concentration of NT on sperm in vivo. Further research is needed to clarify this.

The downstream signaling pathways that might be involved in NT mRNA expression and release were investigated. MAPK, also called mitogen-activated protein kinase, plays an important role in meiotic resumption [44]. Activation of MAPK in cumulus cells induces cumulus expansion by enhancing the expression of hyaluronic acid synthase, which synthesizes hyaluronic acids [45]. The accumulation of hyaluronic acids between cumulus cells physically blocks signal transduction between them, which is considered one of